nature structural & molecular biology

The bacterial dicarboxylate transporter VcINDY uses a two-domain elevator-type mechanism

Christopher Mulligan[1], Cristina Fenollar-Ferrer[2,3], Gabriel A Fitzgerald[1,5], Ariela Vergara-Jaque[2], Desirée Kaufmann[3,5], Yan Li[4], Lucy R Forrest[2] & Joseph A Mindell[1]

Secondary transporters use alternating-access mechanisms to couple uphill substrate movement to downhill ion flux. Most known transporters use a 'rocking bundle' motion, wherein the protein moves around an immobile substrate-binding site. However, the glutamate-transporter homolog Glt_{Ph} translocates its substrate-binding site vertically across the membrane, through an 'elevator' mechanism. Here, we used the 'repeat swap' approach to computationally predict the outward-facing state of the Na^+/succinate transporter VcINDY, from *Vibrio cholerae*. Our model predicts a substantial elevator-like movement of VcINDY's substrate-binding site, with a vertical translation of ~15 Å and a rotation of ~43°. Our observation that multiple disulfide cross-links completely inhibit transport provides experimental confirmation of the model and demonstrates that such movement is essential. In contrast, cross-links across the VcINDY dimer interface preserve transport, thus revealing an absence of large-scale coupling between protomers.

Secondary active transporters constitute a large class of proteins responsible for catalyzing the passage of key compounds across the lipid bilayer in all living cells. These molecular machines harness the energy supplied by the electrochemical gradient of one solute, usually a coupling ion such as H^+ or Na^+, to power the transport of another solute against its concentration gradient. Secondary transporters operate by an alternating-access mechanism in which conformational changes in the protein alternately expose the substrate-binding site to either side of the membrane. A minimum of two conformational states are therefore required to achieve alternating access: an inward-facing state, in which the substrate is accessible to only the cytoplasmic side of the membrane, and an outward-facing state, in which the substrate is accessible to only the extracellular side[1,2]. Many transporters also use intermediate 'occluded' states, in which the substrate-binding site is not accessible to either side of the membrane[3–5].

The ever-growing collection of secondary-transporter crystal structures has revealed a remarkable diversity of protein folds; structural and functional investigations have begun to illuminate the conformational mechanisms by which these folds achieve alternating access. Of the 17 secondary-transporter folds reported to date, the major facilitator superfamily (MFS) fold and the LeuT fold represent a majority of the known protein sequences and an overwhelming majority of the known X-ray crystal structures[6,7]. In both cases, their conformational mechanisms involve movement of helices around a substrate-binding site, which is usually situated at the center of the lipid bilayer. Although the overall mechanism has been described as movements of domains in rocking bundle– or 'rocker switch'–type conformational changes, the available evidence has also suggested a role for individual 'gating' helices that help to determine intermediate steps in the transport cycle[8–12]. Either way, for both of these large families, the substrate retains its relative position in the membrane regardless of the conformation of the transporter.

A dramatically different route to achieving alternating access involves an elevator-type (or 'carrier') mechanism; here, the substrate-binding site itself is moved. Elevator-type transporters are composed of two domains: a scaffold domain, which remains relatively rigid during the transport cycle, and a second domain, referred to as the transport domain, which contains all the residues necessary to bind the substrate. This mechanism derives its name from the elevator-like rigid-body translation of the transport domain back and forth across the hydrophobic barrier provided by the protein and lipid bilayer; this translation is achieved by moving the entirety of the substrate-binding site, thereby allowing the substrate to be alternately exposed to both sides of the membrane. To date, only the glutamate-transporter homolog Glt_{Ph} has been convincingly shown to use an elevator-like mechanism[13,14]. Glt_{Ph} belongs to a relatively small family of proteins (the dicarboxylate/amino acid:cation symporters (DAACS); transporter classification database (TCDB) family 2.A.23), thus raising the possibility that its mechanism is unique to this small family. However, a similar mechanism has recently been hypothesized for the Na^+/H^+ antiporters, although this proposal remains controversial[15]. Thus, the prevalence of elevator-like mechanisms in biology remains a compelling and unanswered puzzle.

[1]Membrane Transport Biophysics Section, National Institute of Neurological Disorders and Stroke, National Institutes of Health, Bethesda, Maryland, USA. [2]Computational Structural Biology Unit, National Institute of Neurological Disorders and Stroke, National Institutes of Health, Bethesda, Maryland, USA. [3]Max Planck Institute of Biophysics, Frankfurt am Main, Germany. [4]Protein/Peptide Sequencing Facility, Porter Neuroscience Research Center, National Institute of Neurological Disorders and Stroke, National Institutes of Health, Bethesda, Maryland, USA. [5]Present addresses: Department of Physiology, Weill Cornell Medical College, New York, New York, USA (G.A.F.), and Institute of Molecular Biology, Mainz, Germany (D.K.). Correspondence should be addressed to L.R.F. (lucy.forrest@nih.gov) or J.A.M. (mindellj@ninds.nih.gov).

Received 28 July 2015; accepted 30 December 2015; published online 1 February 2016; doi:10.1038/nsmb.3166

Here, we sought to determine the transport mechanism of vcINDY. Using structural modeling combined with extensive disulfide cross-linking and biochemical and functional characterization of purified VcINDY from *V. cholerae* (Vc), we report that the Na^+/succinate transporter VcINDY also uses an elevator-type mechanism. VcINDY belongs to the divalent anion/sodium symporter (DASS) family of transporters (TDCB family 2.A.47). This family also contains members of the SLC13 family, which are responsible for the uptake of citrate, Krebs-cycle intermediates and sulfate, in humans[16–18]. VcINDY is the only DASS family member for which a high-resolution structure is known[19]. The 3.2-Å structure of VcINDY reveals a dimeric architecture; the positioning of the bound ligand, in this case citrate, indicates that this structure reflects an inward-facing state of the transporter. Each protomer consists of 11 transmembrane (TM) helices that can be partitioned into two distinct domains: a scaffold domain, which forms all interprotomer contacts, and a transport domain, which houses the substrate-binding site (**Figs. 1** and **2**)—an arrangement highly reminiscent of Glt_{Ph}.

The results presented here computationally predict and experimentally confirm an outward-facing state of VcINDY and indicate that an ~15-Å translation accompanied by an ~43° rigid-body rotation of the transport domain occurs, thus exposing the substrate-binding site to the external solution. This work therefore reveals a second transporter family that has a fold different from that of Glt_{Ph} and that uses an elevator-type mechanism with similarities to that of Glt_{Ph} but also with key differences. Given the relationship between VcINDY and other families in the large ion transporter (IT) superfamily, we suggest that this superfamily shares key features of the elevator mechanism and that, like the rocking bundle–type mechanisms, this conformational strategy is also widespread in secondary transport[20–22].

RESULTS

VcINDY contains inverted-topology structural repeats

For VcINDY, a structure of only the inhibitor-bound, inward-facing state is available[19]. We sought to explore additional conformations of VcINDY through repeat-swap homology modeling, wherein we identified repeating structural units in the crystal structure, then swapped the conformations of these repeating units[23]. The success of this procedure in previous studies has relied on the imperfect symmetry of the structures of the repeating units; any subtle conformational differences between the repeating units can lead to the prediction of alternate conformational states[13,23–26].

VcINDY contains an inverted-topology structural repeat related by pseudo–two-fold symmetry around an axis in the plane of the membrane[19]: repeat unit 1 (RU1), consisting of TM helices 2–6 (defined here as residues 42–242), and repeat unit 2 (RU2), consisting of TM helices 7–11 (residues 260–453; **Fig. 1a**,**b**). TM1 is a peripheral helix in VcINDY and is not part of either repeating unit. Our alignments of the amino acid sequences of RU1 and RU2 revealed a low sequence identity of ~20% (**Supplementary Fig. 1a**). However, superimposition of the repeating units clearly indicated that they share a similar architecture, with an r.m.s. deviation for the Cα atoms of ~4.3 Å (**Fig. 1c**). When we compared only the transport domain or scaffold domain, we found much higher structural similarity (r.m.s. deviations of 2.0–2.1 Å), thus suggesting that the main contribution to the structural differences between the repeats comes from the orientation of the transport-domain helices relative to the scaffold-domain helices (**Fig. 1c**).

Predicting an outward-facing state of VcINDY

We applied the repeat-swap procedure to VcINDY by modeling the conformation of RU1 by using RU2 as a template, and vice versa (**Figs. 1** and **2a** and **Supplementary Fig. 1b**). The resulting model revealed a substantial conformational change compared to the inward-facing crystal structure (**Fig. 2b**). As a result of this conformational change, which involves movements of the transport domain relative to the scaffold domain, the substrate-binding site becomes exposed to the extracellular side of the membrane; thus, the repeat-swapped model clearly represents a putative outward-facing state of VcINDY (**Fig. 2c** and **Supplementary Fig. 2**).

To analyze the conformational changes that occur during the transformation from the inward- to the outward-facing conformation, we superimposed the model onto the structure by using only helices from the oligomerization interface; this also allowed us to construct a model of the dimer (**Fig. 2b**). Our dimer model is therefore based on the assumption that the dimer interface is unchanged during transport (tested explicitly below). Comparison of the two states predicted that the entire transport domain undergoes an ~15-Å

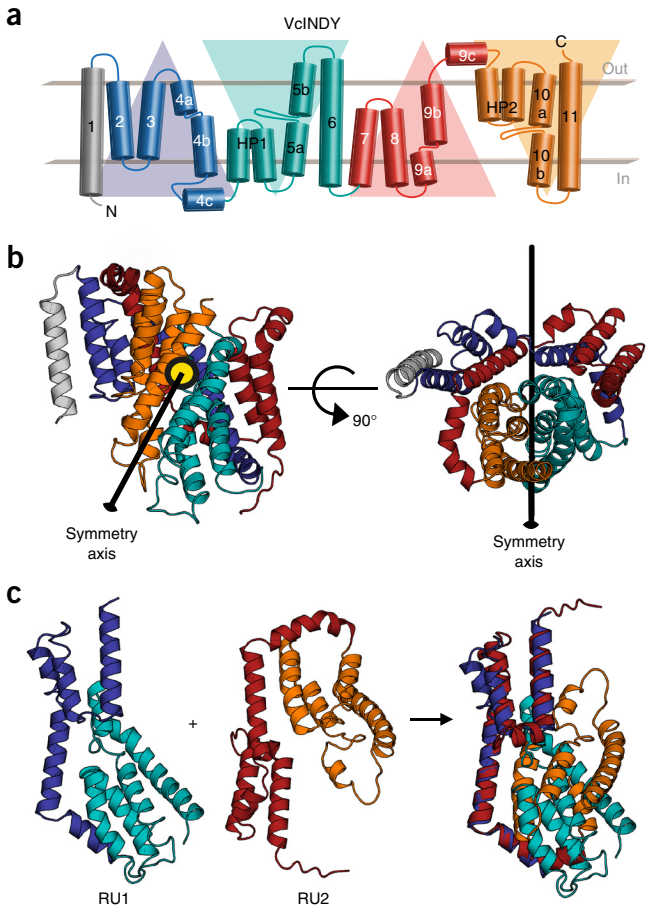

Figure 1 Repeat-swap modeling of VcINDY. (**a**) Schematic representation of the topology of VcINDY, colored according to the structural repeats. Blue and cyan helices compose repeat unit 1 (RU1), and red and orange helices compose repeat unit 2 (RU2). (**b**) Cartoon representation of the X-ray crystal structure of a VcINDY protomer, showing that RU1 is related to RU2 by two-fold pseudosymmetry, with the symmetry axis parallel to the membrane. The VcINDY protomer is viewed from within the plane of the membrane (left) and from the extracellular side of the protein (right). (**c**) Cartoon representation showing a structural alignment, built with TM-Align, of the repeats with the helices colored according to the topology in **a**. The initial sequence alignment used to build a swapped-repeat model was generated on the basis of this structural alignment.

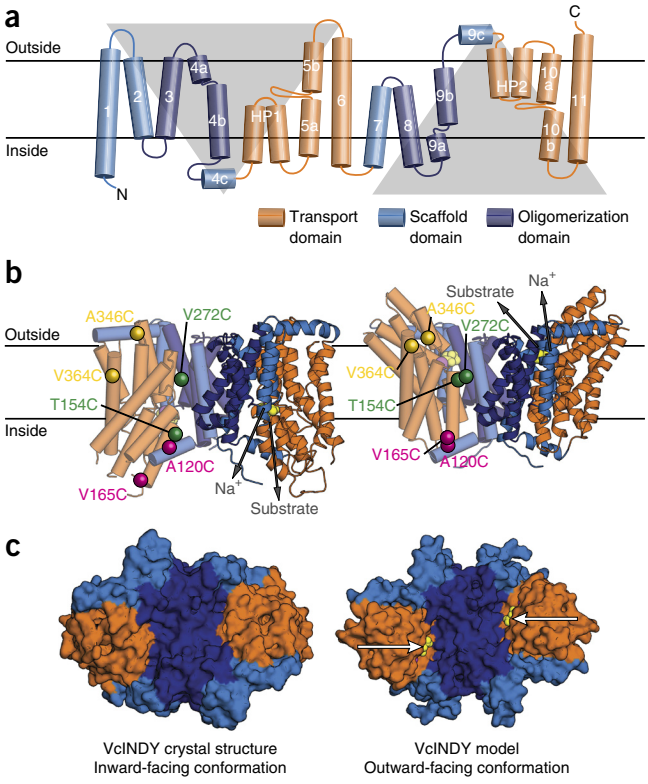

Figure 2 Predicted VcINDY conformational change. (**a**) Topology diagram of a VcINDY protomer colored according to the helices forming the scaffold (light blue), oligomerization (dark blue) and transport (orange) domains. Gray triangles indicate RU1 (downward-pointing triangle) and RU2 (upward-pointing triangle). (**b**) Cartoon representation of the dimeric VcINDY X-ray crystal structure in an inward-facing conformation (left) and the model in an outward-facing conformation (right) viewed from the membrane plane. Substrate and Na^+ are shown as spheres, with their pathways indicated by gray arrows. Cα atoms of the residues studied by cross-linking are shown as spheres colored in pairs (left-hand protomers). (**c**) Surface representation of the VcINDY X-ray crystal structure (left) and model (right) viewed from the extracellular side. The substrate (yellow spheres, indicated by arrows) is visible from the extracellular side in the model (right) but not in the inward-facing crystal structure (left).

vertical translation accompanied by an ~43° rotation as it transitions from inward- to outward-facing states (**Supplementary Fig. 2** and **Supplementary Movie 1**).

Design of cysteine pairs to test the outward-facing model

The outward-facing model suggests that transport requires a major translocation of the transport domain, accompanied by a significant rotation. If such a motion indeed occurs, then there should be residues that are far apart in one state but that are brought into proximity in the other state. We tested this idea by introducing pairs of cysteine residues at positions that are widely separated in the inward-facing structure (Cβ-Cβ distance >12 Å) but are brought closely enough together (Cβ-Cβ distance <7 Å) in the predicted outward-facing state that they could potentially form disulfide links. We predicted that cross-linking these residue pairs should confine the protein to a single state in the transport cycle, thereby strongly inhibiting transport. To validate this approach, we also designed a cysteine pair that should selectively stabilize the known inward-facing state, by substituting residues that are distant in the outward-facing model but in proximity in the inward-facing crystal structure.

As a starting construct, we used a mutant in which the three native cysteines were replaced with serine. This protein effectively catalyzed Na^+-driven succinate uptake (**Supplementary Fig. 3a**). From 18 candidate pairs, we selected three double mutants for further examination: T154C V272C, A120C V165C and A436C V364C (distances in Online Methods). Together, these cysteine pairs occupy three different positions at the interface between the transport and scaffold domains, thus providing good coverage of the conformational change predicted by our model. To stabilize the inward-facing state, we introduced the double-cysteine mutant L60C S381C (**Supplementary Fig. 4a**). All four cysteine pairs were well tolerated by VcINDY (**Supplementary Fig. 3b**) and demonstrated robust transport activity (described below).

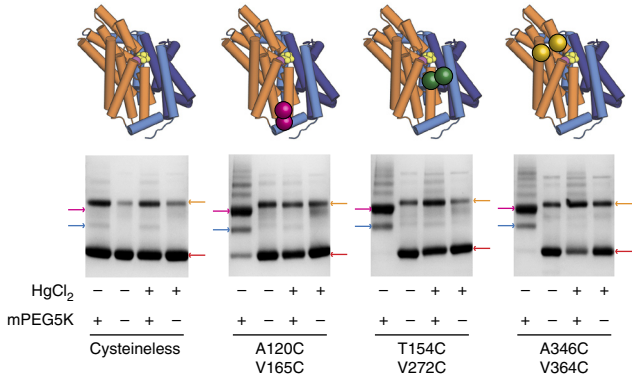

Cysteine cross-linking supports the outward-facing model

We screened for successful cross-links by using the gel-shift assay described by Basilio *et al.*[27], using either $HgCl_2$, which can act as a homobifunctional cross-linking reagent, or the oxidizing agent copper phenanthroline (CuPhen) to catalyze disulfide-bond formation. Specifically, after treatment with cross-linker, we enumerated the remaining free cysteines by treating the protein with 5-kDa PEG-maleimide (mPEG5K), which causes a substantial shift in the protein's gel mobility upon reaction with free cysteine. If the introduced cysteines are cross-linked with each other, however, then they will be unable to react with mPEG5K, and the protein band will run as monomeric VcINDY on SDS-PAGE. Before cross-linking, each double-cysteine mutant was almost completely PEGylated after incubation with mPEG5K, thus demonstrating that both cysteines were accessible to the probe (**Fig. 3** and **Supplementary Fig. 4b**). In contrast, after treatment with cross-linker, all three outward-stabilizing double-cysteine mutants (**Fig. 3** and **Supplementary Fig. 5**) and the inward-stabilizing mutant (**Supplementary Fig. 4b**) were completely protected from PEGylation, thus suggesting that all four double mutants successfully formed intramolecular cross-links.

Figure 3 Chemical cross-linking of outward-stabilizing cysteine pairs. SDS-PAGE band-shift assay showing the number of free cysteines present in cysteineless VcINDY and three double-cysteine mutants (A120C V165C; T154C V272C; and A346C V364C) with (+) and without (–) prior treatment with $HgCl_2$. Relative positions of the cysteine pairs are shown in the cartoon representation of a VcINDY protomer (top). The following protein species seen in the gels are indicated by colored arrows; unmodified VcINDY (red arrows), dimeric VcINDY (orange arrows), singly PEGylated VcINDY (blue arrows) and doubly PEGylated VcINDY (magenta arrows). Nonreducing SDS-PAGE gels with protein visualized with Coomassie dye are shown. The assay was performed on at least two separate occasions with the same outcome. Original images of gels and blots used in this study can be found in **Supplementary Data Set 1**.

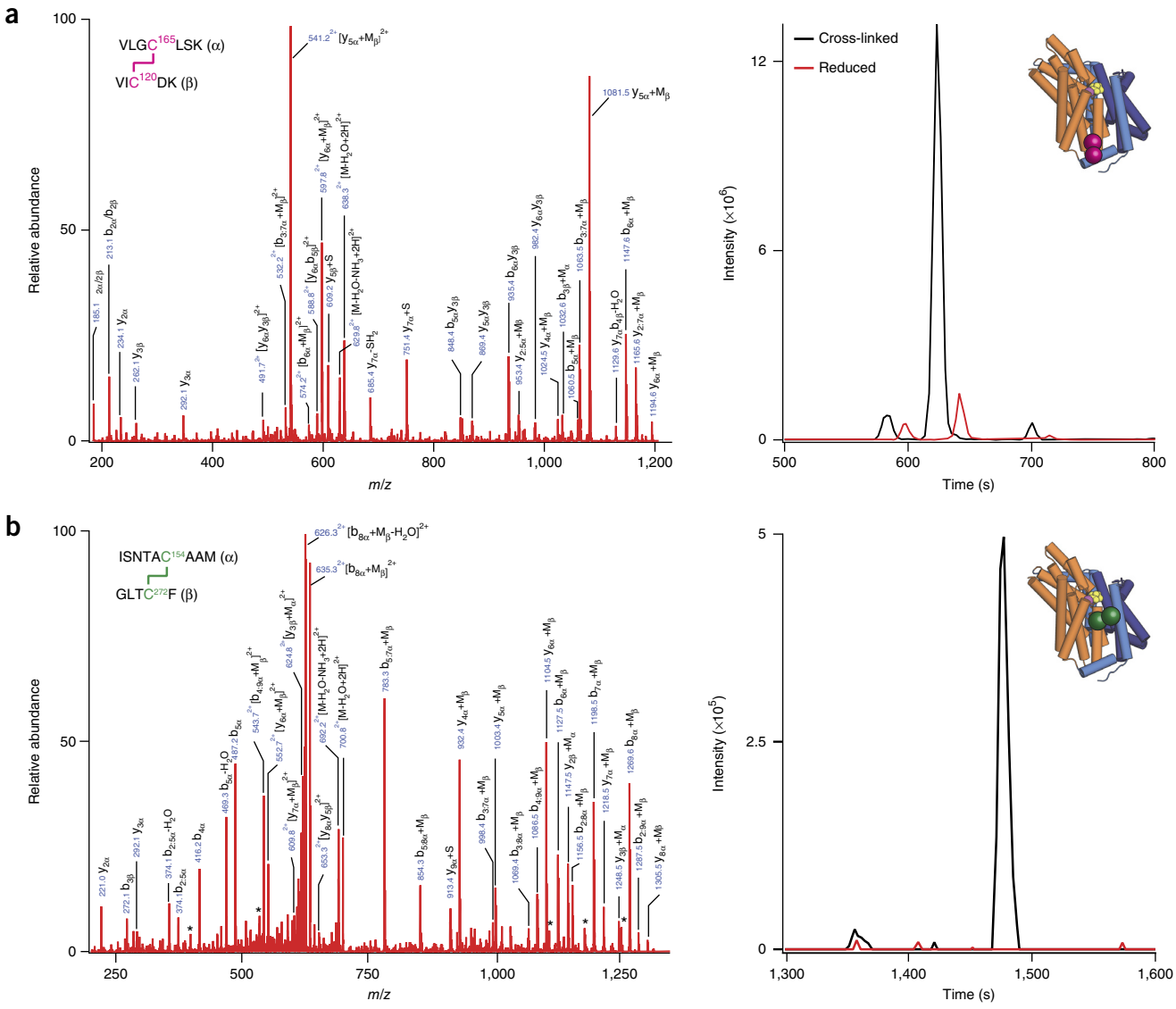

Figure 4 MS identification of cross-linked peptides. (**a**,**b**) Representative LC-MS/MS spectra of disulfide-linked peptides detected from the digests of CuPhen-treated A120C V165C (**a**) and T154C V272C (**b**). Collision-induced dissociation (CID) spectrum of the disulfide-linked peptide (inset) from the proteolytic digests (left) and the associated extracted ion chromatogram (right) for protein treated with cross-linking reagent (black line) or maintained in reducing conditions (red line). This experiment was repeated twice with separately prepared and treated protein. The annotation *i:j* represents fragments from internal cleavage; for example, y2:5 represents the peptide fragment from the second to the fifth residue. Asterisks represent fragments with a neutral loss of water.

Treatment of the double-cysteine mutants with cross-linking reagents did not significantly affect the elution volume of the protein peak in size-exclusion chromatography (SEC) but did result in slight peak broadening; we observed minimal aggregation of these proteins (data not shown). Treating the six single-cysteine mutants with either Hg^{2+} or CuPhen revealed proteins running primarily as monomers on SDS PAGE (**Supplementary Fig. 6**). Several single-cysteine mutants, for example, V364C and V165C, showed some dimerization in the presence of $HgCl_2$; however, the lack of dimerization observed in double mutants containing these same mutations further supported the conclusion that intramolecular disulfide bridges had formed between the introduced cysteines and not between protomers. These results indicated that treatment with cross-linking reagent was well tolerated and that the fold of the cross-linked protein remained intact.

To obtain direct physical evidence of cross-link formation, we analyzed the double-cysteine mutants through LC-MS/MS (**Fig. 4**). If cross-links indeed formed in the cysteine mutants, then cross-linked peptides should be directly detected through this approach. After incubating the cysteine mutants with either CuPhen or dithiothreitol (DTT; to prevent spontaneous cross-link formation), we digested the proteins and acquired MS and MS/MS spectra of the resulting peptides. We identified the expected disulfide-cross-linked peptides in the CuPhen-treated samples of both A120C V165C and T154C V272C (**Fig. 4**); these peptides were completely absent in the reduced protein samples (**Fig. 4a**,**b**). We also detected a peptide that was consistent with cross-link formation between A346C and V364C. However, the size of the peptide and the quality of the MS/MS spectra prevented us from confidently assigning the MS fragment peaks (data not shown). Because of the same technical limitation, we were also unable to obtain consistent LC-MS/MS data for the inward-stabilizing mutant L60C S381C. As a negative control for cross-link formation, we performed MS on the A120C V364C mutant, in which the cysteines should never be close enough to form

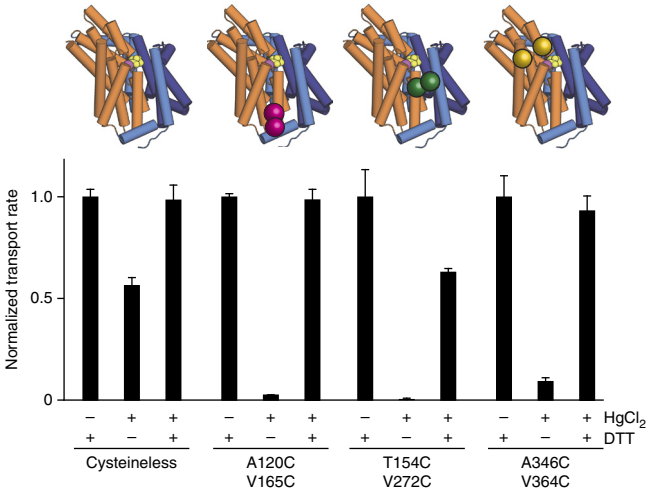

Figure 5 Stabilizing VcINDY in the outward-facing state abolishes transport. Normalized initial rates of [^{3}H]succinate transport in the presence of proteoliposomes containing cysteineless VcINDY or three double-cysteine mutants compatible with the outward-facing state after treatment with (+) and without (–) $HgCl_2$ and DTT. Relative positions of cysteine pairs are shown as in **Figure 3**. Results from triplicate data sets are shown. Error bars, s.e.m. This experiment was repeated twice with fresh preparations of proteoliposomes.

a disulfide bond. For this protein, we observed no evidence of cross-link formation in the MS experiments, nor was the 120C-containing peptide depleted from the spectra, thus confirming that these cysteines (which are distant in either structure) do not react with each other (again, the 364C peptide was difficult to observe for technical reasons). These data unequivocally demonstrated cross-link formation between two of the introduced cysteine pairs and suggested that the mPEG5K labeling results for the other two pairs indeed reflected cross-link formation. Formation of these cross-links supports our prediction that the outward-facing conformation of VcINDY requires a specific, large excursion of the transport domain (**Supplementary Movie 2**).

Cross-linking VcINDY abolishes transport activity

Our hypothesis for the VcINDY transport mechanism, based on the model of the outward-facing conformation, is that the translocation of the transport domain is essential for transport and functions by physically moving the binding site from one side of the membrane to the other (**Fig. 2** and **Supplementary Movie 1**). If true, then cross-linking VcINDY in either the inward- or outward-facing state should straitjacket the transporter and curtail its transport activity. We tested this prediction by reconstituting the double-cysteine mutants into proteoliposomes and measuring succinate-transport activity in the presence or absence of a disulfide link (**Fig. 5**). Indeed, when we formed cross-links by treating proteoliposomes containing double-cysteine mutants with excess $HgCl_2$ (on both sides of the membrane) we observed almost-complete cessation of succinate-transport activity for all three outward-stabilizing cysteine mutants (**Fig. 5**) and for the inward-stabilizing mutant (**Supplementary Fig. 4c**). Transport activity was almost completely restored (except in the case of T154C V272C, which regained ~60% of its transport activity) when the cross-links were reduced, thus indicating that the abolition of transport was caused by disulfide-bond formation. The retention of substantial transport activity in the $HgCl_2$-treated cysteineless protein confirmed that the strong inhibition in the cross-linked proteins was due to the specific effects of the cross-linking agents on the double-cysteine mutants. Together, these results support our hypothesis that the large conformational change required to form the cross-links is also an essential component of the transport process.

Rigidity of the dimer interface during transport

The data described thus far demonstrated large-scale conformational changes between helices in the scaffold and helices in the transport domain. In constructing a model of the outward-facing dimer, as described above, we assumed that the helices contributing to the oligomerization interface (i.e., those from the scaffold) remained fixed relative to one another. We tested this assumption by assessing the functional effects of 'stapling' the protomers together at several interprotomer contact points[28]. If substantial conformational changes at the dimer interface are essential for transport, then stapling the protein at these positions should abolish transport activity.

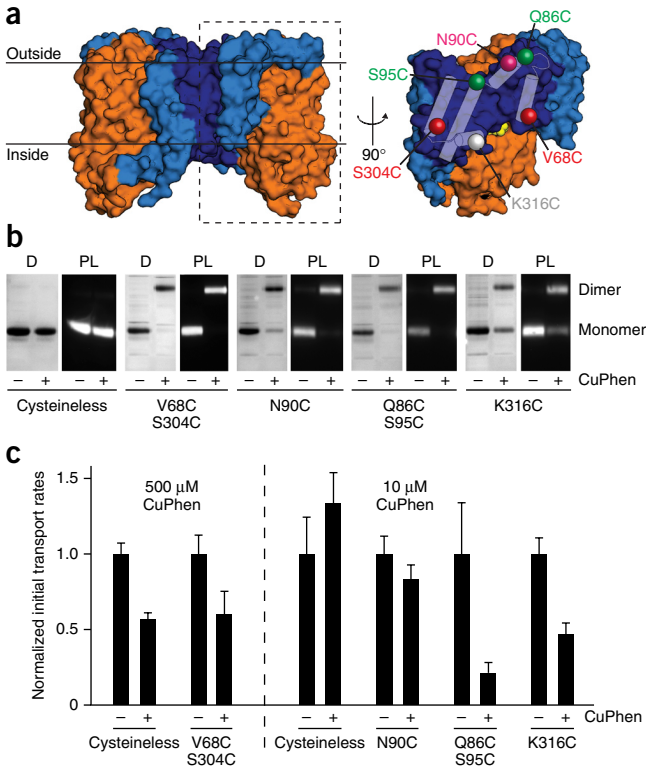

Figure 6 Constraining the dimer interface has minimal effects on transport. (**a**) Surface representation of a VcINDY dimer viewed from the plane of the membrane (left) and a VcINDY protomer viewed from the dimer interface (right), if the VcINDY dimer is opened like a book. Cylinders represent the interfacial α-helices that make the intraprotomer contacts across the dimer interface. The colored spheres represent the positions of cysteine residues introduced to staple the VcINDY protomers together. (**b**) Coomassie-stained SDS-PAGE gels of purified cysteine mutants in detergent solution (D) and histidine-tag western blot analysis of VcINDY-containing proteoliposomes (PL), with (+) and without (–) treatment with CuPhen. The positions of monomeric and dimeric VcINDY are indicated. (**c**) Normalized initial transport rates of cysteineless VcINDY and indicated cysteine mutants with (+) and without (–) treatment with CuPhen (at the indicated concentrations). Results are from two independent experiments with three technical replicates each. Error bars, s.e.m. Western blots were performed three separate times, and transport assays were repeated at least twice with the same outcome. Original images of gels and blots used in this study can be found in **Supplementary Data Set 1**.

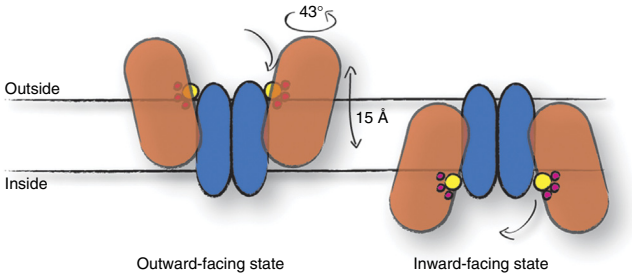

Figure 7 Proposed elevator-type transport mechanism in the VcINDY dimer. Cartoon representation of the transport mechanism inferred from the inward-facing crystal structure and outward-facing model of VcINDY. Blue shapes represent the scaffold and oligomerization domains, and the orange shape is the transport domain. Substrates are represented by yellow spheres (succinate) and pink spheres (Na^+ ions). In our scheme, the substrates bind the outward-facing state of VcINDY (left, model) at which point the transport domain undergoes an ~15 Å translocation and an ~43° rotation into the inward-facing state (right, crystal structure), which allows substrate to be released into the cytoplasm. The empty transporter must then recycle back to the outward-facing state to restart the cycle.

We introduced cysteine pairs into the dimer interface at four contact points (**Fig. 6a**): Q86C (helix 4a) and S95C (TM4b); V68C (TM3) and S304C (TM8); N90C (helix 4a); and K316C (TM9). Because of the two-fold symmetry of the VcINDY homodimer, we expected the mutants containing two cysteine residues per protomer to form two disulfide bonds across the interface, whereas we expected the single-cysteine mutants to form single disulfide bonds (with their symmetry-related counterparts in the other protomer). Each interfacial cysteine mutant was stable and exhibited transport activity when reconstituted into liposomes (**Fig. 6** and **Supplementary Fig. 7**).

Interprotomer cross-links formed readily upon incubation with CuPhen, as reflected by a shift of the protein band from the monomeric VcINDY molecular weight to that expected for the dimer in SDS-PAGE, and they remained stable upon reconstitution into proteoliposomes (**Fig. 6b**). Incubation with 10 µM 2:1 CuPhen for 45 min at room temperature fully cross-linked all proteins except for the V68C S304C mutant. V68C S304C required 500 µM CuPhen to attain full cross-linking, which presumably reflects reduced accessibility of these residues to the cross-linking agent or suboptimal alignment of the two cysteines.

All four stapled mutants still transported succinate after cross-link formation (**Fig. 6c**), thus demonstrating that there are no substantial conformational changes in these positions that are essential for transport (**Fig. 6c**). However, the functional effects of stapling the dimer interface varied depending on the position of the disulfide cross-link. Cross-linking two of the mutants, V68C S304C and N90C, had no discernible effect on transport activity beyond the nonspecific effects that we observed for cysteineless VcINDY (**Fig. 6c**; discussion of the effects of reducing agents on activity in Online Methods). Interestingly, however, cross-linking the other two mutants, Q86C S95C and K316C, resulted in five-fold and two-fold decreases in transport activity, respectively. A possible explanation is that the cross-linking causes a local distortion in the scaffold domain that reduces the ability of the transport domain to move along it, or that transport is facilitated by some movement within the dimer interface that is impeded by the cross-link. Further experiments will be necessary to illuminate the underlying causes of these more subtle effects.

DISCUSSION

In this study, we present a structural model of the outward-facing state of VcINDY along with extensive supporting experimental data. This work demonstrates that VcINDY uses an elevator-type movement, with protein excursions on the order of ~15 Å, that is an essential step in the transport cycle. The formation of disulfide cross-links in three different locations, each physically separated in the inward-facing structure but predicted by our model to be juxtaposed in the outward-facing state, showed that the protein can adopt the predicted outward-facing conformation. That the cross-links profoundly disrupted transport confirmed that movement to and from this state is essential for transport. In contrast, preservation of transport activity in the presence of cross-links across the dimer interface revealed that no major conformational change in this region is required for activity.

Because repeat-swap modeling is, in essence, a homology modeling technique, the error of the model depends on the difference in the sequences of the two repeats; in the case of VcINDY, the two repeats contain ~20% identical residues, thus implying a structural error of 1–3 Å in the Cα positions[26,29,30]. However, our updated protocol reduced this error significantly, by including a second refinement step that effectively maintained the integrity of the domains moving relative to one another, while preserving the overall movement of those domains (Online Methods and **Supplementary Figs. 2** and **7**). Our results suggest that the transport domain moves vertically ~15 Å and rotates ~43°, thereby translocating the substrate-binding site to the other side of the hydrophobic barrier provided by TM helices 4 and 9 (**Fig. 7**). Insofar as the X-ray structure represents an actual inward-facing state of VcINDY, we expect our model to accurately represent the outward-facing state. However, as discussed previously[26], if the structure does not represent the true inward-facing state, we expect our model to deviate accordingly. The success of our experimental test of the model, with multiple cross-links capturing the outward-facing state, suggests that the modeled conformation represents a native state, with errors of a few angstroms, and that the conformational change is truly elevator like.

A key assumption underlying our results is that the states stabilized by our cross-links represented well-populated conformations accessible to the native protein rather than rarely visited grotesques that had been kinetically trapped by the disulfide bond. We report cross-links between three different cysteine pairs, distributed across the transport domain–scaffold domain interface. This combination of appositions would be extraordinarily difficult to achieve with a fundamentally different conformational change. Moreover, the wide range of conditions used in these experiments, including cross-link formation with either CuPhen or $HgCl_2$ and with protein in either detergent or lipid membranes, suggested that we sampled a native state of the protein. In addition, the consistent mobility of the cross-linked protein in SEC ruled out the possibility of a reversibly denatured form of the protein that was stabilized by the cross-link.

How does the movement of VcINDY compare with other proposed elevator-type transporters? Until very recently, the only transporter that could indisputably be called an elevator-type transporter was the glutamate-transporter homolog, Glt_{Ph}[14,31]. Our results demonstrated that the transport domain of VcINDY undergoes a similar perpendicular and rotational movement to that of Glt_{Ph} (~15 Å and 43° for VcINDY versus 16 Å and 37° for Glt_{Ph})[14]. Structures of the citrate/sodium symporter SeCitS from *Salmonella enterica* have very recently been reported, while this work was in revision, and have revealed a second clear example of an elevator mechanism[32]. In this

case, the conformational change is an ~16 Å translation and a 31° rotation of the transport domain. The fold of CitS differs from that of VcINDY in that the helical hairpin follows the unbroken helix in each repeat of CitS rather than preceding it, as it does in VcINDY. However, the two structures share a common arrangement of scaffold and transport domains, thus providing additional support to the mechanism for VcINDY reported here.

Recently, it has been suggested that members of the cation-proton antiporter (CPA) family, exemplified by the Na^+/H^+ exchanger NhaA, use an elevator-type mechanism, although this remains controversial. Several lines of evidence, both theoretical and experimental, have suggested that in *Escherichia coli* NhaA, a panel of four TM helices rotate within the plane of the membrane to open and close the inward- and outward-facing pathways[25]. However, a recent structural comparison of NhaA with NapA, a remote homolog, has been interpreted as being consistent with an elevator-type movement[15]. However, NapA shares <15% identical residues with NhaA, thus casting doubt on any conclusions based on this direct comparison. Furthermore, more recent structural analysis of two other CPA family members, PaNhaP from *Pyrococcus abyssi* and MjNhaP1 from *Methanocaldococcus jannaschii*, have suggested that only slight conformational changes are required for transport[33,34]. The structure of a bacterial concentrative nucleoside transporter, VcCNT, has also revealed the hallmarks of an elevator-type transporter, although the structure of VcCNT has been captured in only an inward-facing state to date[35,36]. Interestingly, repeat-swap modeling of VcCNT has predicted an elevator-type movement for this protein, though this prediction has not yet been experimentally tested[26].

Several shared structural features are immediately apparent in the structures of Glt_{Ph}, VcINDY and VcCNT. All three transporters have a similar overall architecture, with a scaffold domain wrapped around a transport domain, and all are oligomers (VcINDY is a dimer, and Glt_{Ph} and VcCNT are trimers), possibly to aid in stabilization. In all three cases, the transport domain contains two reentrant hairpin loops that dip into the membrane but do not cross it: the tips of these reentrant loops coordinate substrates in all three transporters. Finally, all three folds contain a broken helix whose two segments are connected through an intramembrane loop (helices 5 and 10 in VcINDY; **Fig. 2a**) that also contributes to the substrate-binding region.

A major mechanistic difference between Glt_{Ph} and VcINDY is seemingly that in Glt_{Ph} the reentrant hairpin loops act as inner and outer gates that cover the substrate-binding site and regulate substrate binding and release. In both the inward-facing structure and the outward-facing model of VcINDY, the substrate is almost completely solvent exposed (**Fig. 2**), thus obviating the need for such gate movement. However, the electron density in the VcINDY crystal structure is ascribed to citrate, which is, in fact, a low-affinity inhibitor[17]. Thus, our current analysis of the inhibitor-bound structure and model may miss some more subtle structural changes, for example, gate movement.

Recent reports have provided evidence that several transporter families have essentially the same fold as VcINDY[22,37]. These transporters include the human Na^+ P_i transporter, NaPi-II[37], and two recently structurally characterized representatives from the *p*-aminobenzoylglutamate transporter (AbgT) family, YdaH and MtrF[22,38,39]. The DASS family, to which VcINDY belongs, and the AbgT family are both members of the IT superfamily, thus suggesting that the elevator-type movement is a common mechanism for all IT superfamily members. Clearly, the mechanism underlying transport by the other IT superfamily members must be investigated, but the commonality of this architecture hints at the widespread use of this mechanism.

Mammalian homologs of VcINDY are potential drug targets in the treatment of metabolic diseases, age-related diabetes and obesity[16,40]. VcINDY is ~30% identical and shares a number of functional characteristics, such as substrate specificity and coupling-ion stoichiometry, with its mammalian homologs, particularly hNaDC3 (ref. 17). In addition, both VcINDY and hNaDC3 are allosterically inhibited by the anthranilic acid derivative flufenamic acid, which is thought to interact at the interface between the scaffold and the transport domain[17,41,42]. These fundamental mechanistic similarities suggest that the overall architecture and basic mechanism of transport are similar in all members of the DASS family. By extension, it would appear that the elevator-type motion is also an essential part of the transport cycle in the mammalian counterparts. Further work is required to explicitly demonstrate a shared conformational mechanism for this family of transporters.

Why would the elevator-type mechanism be favored over other transport mechanisms such as the rocking-bundle mechanism? One apparently common characteristic of several potential elevator-type transporters is the tendency to couple substrate transport to multiple (three or more) coupling ions. At equilibrium, increasing the number of coupling ions (n) dramatically increases the capacity for substrate accumulation, and this increase changes as the nth power of the ion gradient. We speculate that an elevator mechanism might be a useful way to insulate the transporter from back-leakage of substrate or coupling ions because, in contrast with rocking-bundle transporters, it can never contain a continuous return path.

METHODS

Methods and any associated references are available in the online version of the paper.

Accession codes. The outward-facing-dimer model has been submitted to the Protein Model Database under identifier PM0080216 and is also available in the online version of the paper as **Supplementary Data Set 2**.

Note: Any Supplementary Information and Source Data files are available in the online version of the paper.

ACKNOWLEDGMENTS

We thank A. Banerjee for helpful discussions and M. Maduke, J. Faraldo-Gómez, G. Rudnick and M. Mayer for critical review of the manuscript. A.V.-J. is supported as a recipient of the L'Oreal Chile–United Nations Educational, Scientific and Cultural Organization (UNESCO) Women in Science Fellowship and the L'Oreal-UNESCO Rising Talent Award. This work was supported by the Division of Intramural Research of the US National Institutes of Health, National Institute of Neurological Disorders and Stroke.

AUTHOR CONTRIBUTIONS

L.R.F. and J.A.M. conceived the project. C.F.-F., A.V.-J. and D.K. carried out computational modeling, and C.F.-F. and L.R.F. analyzed data and directed computational modeling efforts. J.A.M. and C.M. designed and planned experiments. C.M. performed experiments and supervised G.A.F., who performed dimer-interface experiments. Y.L. performed MS and interpreted MS data. C.M., C.F.-F., L.R.F. and J.A.M. wrote the manuscript.

COMPETING FINANCIAL INTERESTS

The authors declare no competing financial interests.

1. Jardetzky, O. Simple allosteric model for membrane pumps. *Nature* **211**, 969–970 (1966).
2. Mitchell, P. A general theory of membrane transport from studies of bacteria. *Nature* **180**, 134–136 (1957).
3. Boudker, O., Ryan, R.M., Yernool, D., Shimamoto, K. & Gouaux, E. Coupling substrate and ion binding to extracellular gate of a sodium-dependent aspartate transporter. *Nature* **445**, 387–393 (2007).

4. Krishnamurthy, H., Piscitelli, C.L. & Gouaux, E. Unlocking the molecular secrets of sodium-coupled transporters. *Nature* **459**, 347–355 (2009).
5. Yamashita, A., Singh, S.K., Kawate, T., Jin, Y. & Gouaux, E. Crystal structure of a bacterial homologue of Na^+/Cl^--dependent neurotransmitter transporters. *Nature* **437**, 215–223 (2005).
6. Reddy, V.S., Shlykov, M.A., Castillo, R., Sun, E.I. & Saier, M.H. Jr. The major facilitator superfamily (MFS) revisited. *FEBS J.* **279**, 2022–2035 (2012).
7. Västermark, Å. & Saier, M.H. Jr. Evolutionary relationship between 5+5 and 7+7 inverted repeat folds within the amino acid-polyamine-organocation superfamily. *Proteins* **82**, 336–346 (2014).
8. Fowler, P.W. *et al.* Gating topology of the proton-coupled oligopeptide symporters. *Structure* **23**, 290–301 (2015).
9. Kazmier, K., Sharma, S., Islam, S.M., Roux, B. & Mchaourab, H.S. Conformational cycle and ion-coupling mechanism of the Na^+/hydantoin transporter Mhp1. *Proc. Natl. Acad. Sci. USA* **111**, 14752–14757 (2014).
10. Kazmier, K. *et al.* Conformational dynamics of ligand-dependent alternating access in LeuT. *Nat. Struct. Mol. Biol.* **21**, 472–479 (2014).
11. Krishnamurthy, H. & Gouaux, E. X-ray structures of LeuT in substrate-free outward-open and apo inward-open states. *Nature* **481**, 469–474 (2012).
12. Shimamura, T. *et al.* Molecular basis of alternating access membrane transport by the sodium-hydantoin transporter Mhp1. *Science* **328**, 470–473 (2010).
13. Crisman, T.J., Qu, S., Kanner, B.I. & Forrest, L.R. Inward-facing conformation of glutamate transporters as revealed by their inverted-topology structural repeats. *Proc. Natl. Acad. Sci. USA* **106**, 20752–20757 (2009).
14. Reyes, N., Ginter, C. & Boudker, O. Transport mechanism of a bacterial homologue of glutamate transporters. *Nature* **462**, 880–885 (2009).
15. Lee, C. *et al.* A two-domain elevator mechanism for sodium/proton antiport. *Nature* **501**, 573–577 (2013).
16. Bergeron, M.J., Clémençon, B., Hediger, M.A. & Markovich, D. SLC13 family of Na^+-coupled di- and tri-carboxylate/sulfate transporters. *Mol. Aspects Med.* **34**, 299–312 (2013).
17. Mulligan, C., Fitzgerald, G.A., Wang, D.N. & Mindell, J.A. Functional characterization of a Na^+-dependent dicarboxylate transporter from *Vibrio cholerae*. *J. Gen. Physiol.* **143**, 745–759 (2014).
18. Saier, M.H. Jr., Tran, C.V. & Barabote, R.D. TCDB: the Transporter Classification Database for membrane transport protein analyses and information. *Nucleic Acids Res.* **34**, D181–D186 (2006).
19. Mancusso, R., Gregorio, G.G., Liu, Q. & Wang, D.N. Structure and mechanism of a bacterial sodium-dependent dicarboxylate transporter. *Nature* **491**, 622–626 (2012).
20. Chen, J.S. *et al.* Phylogenetic characterization of transport protein superfamilies: superiority of SuperfamilyTree programs over those based on multiple alignments. *J. Mol. Microbiol. Biotechnol.* **21**, 83–96 (2011).
21. Prakash, S., Cooper, G., Singhi, S. & Saier, M.H. Jr. The ion transporter superfamily. *Biochim. Biophys. Acta* **1618**, 79–92 (2003).
22. Vergara-Jaque, A., Fenollar-Ferrer, C., Mulligan, C., Mindell, J.A. & Forrest, L.R. Family resemblances: a common fold for some dimeric ion-coupled secondary transporters. *J. Gen. Physiol.* **146**, 423–434 (2015).
23. Forrest, L.R. *et al.* Mechanism for alternating access in neurotransmitter transporters. *Proc. Natl. Acad. Sci. USA* **105**, 10338–10343 (2008).
24. Radestock, S. & Forrest, L.R. The alternating-access mechanism of MFS transporters arises from inverted-topology repeats. *J. Mol. Biol.* **407**, 698–715 (2011).
25. Schushan, M. *et al.* A model-structure of a periplasm-facing state of the NhaA antiporter suggests the molecular underpinnings of pH-induced conformational changes. *J. Biol. Chem.* **287**, 18249–18261 (2012).
26. Vergara-Jaque, A., Fenollar-Ferrer, C., Kaufmann, D. & Forrest, L.R. Repeat-swap homology modeling of secondary active transporters: updated protocol and prediction of elevator-type mechanisms. *Front. Pharmacol.* **6**, 183 (2015).
27. Basilio, D., Noack, K., Picollo, A. & Accardi, A. Conformational changes required for H^+/Cl^- exchange mediated by a CLC transporter. *Nat. Struct. Mol. Biol.* **21**, 456–463 (2014).
28. Groeneveld, M. & Slotboom, D.J. Rigidity of the subunit interfaces of the trimeric glutamate transporter GltT during translocation. *J. Mol. Biol.* **372**, 565–570 (2007).
29. Forrest, L.R., Tang, C.L. & Honig, B. On the accuracy of homology modeling and sequence alignment methods applied to membrane proteins. *Biophys. J.* **91**, 508–517 (2006).
30. Olivella, M., Gonzalez, A., Pardo, L. & Deupi, X. Relation between sequence and structure in membrane proteins. *Bioinformatics* **29**, 1589–1592 (2013).
31. Yernool, D., Boudker, O., Jin, Y. & Gouaux, E. Structure of a glutamate transporter homologue from *Pyrococcus horikoshii*. *Nature* **431**, 811–818 (2004).
32. Wöhlert, D., Grötzinger, M.J., Kühlbrandt, W. & Yildiz, Ö. Mechanism of Na^+-dependent citrate transport from the structure of an asymmetrical CitS dimer. *eLife* **4**, e09375 (2015).
33. Paulino, C., Wöhlert, D., Kapotova, E., Yildiz, Ö. & Kühlbrandt, W. Structure and transport mechanism of the sodium/proton antiporter MjNhaP1. *eLife* **3**, e03583 (2014).
34. Wöhlert, D., Kühlbrandt, W. & Yildiz, O. Structure and substrate ion binding in the sodium/proton antiporter PaNhaP. *eLife* **3**, e03579 (2014).
35. Johnson, Z.L., Cheong, C.G. & Lee, S.Y. Crystal structure of a concentrative nucleoside transporter from *Vibrio cholerae* at 2.4 Å. *Nature* **483**, 489–493 (2012).
36. Johnson, Z.L. *et al.* Structural basis of nucleoside and nucleoside drug selectivity by concentrative nucleoside transporters. *eLife* **3**, e03604 (2014).
37. Fenollar-Ferrer, C. *et al.* Structural fold and binding sites of the human Na^+-phosphate cotransporter NaPi-II. *Biophys. J.* **106**, 1268–1279 (2014).
38. Bolla, J.R. *et al.* Crystal structure of the *Alcanivorax borkumensis* YdaH transporter reveals an unusual topology. *Nat. Commun.* **6**, 6874 (2015).
39. Su, C.C. *et al.* Structure and function of *Neisseria gonorrhoeae* MtrF illuminates a class of antimetabolite efflux pumps. *Cell Rep.* **11**, 61–70 (2015).
40. Colas, C., Pajor, A.M. & Schlessinger, A. Structure based identification of inhibitors for the SLC13 family of Na^+/dicarboxylate cotransporters. *Biochemistry* **54**, 4900–4908 (2015).
41. Burckhardt, B.C., Lorenz, J., Burckhardt, G. & Steffgen, J. Interactions of benzylpenicillin and non-steroidal anti-inflammatory drugs with the sodium-dependent dicarboxylate transporter NaDC-3. *Cell. Physiol. Biochem.* **14**, 415–424 (2004).
42. Pajor, A.M. & Sun, N.N. Nonsteroidal anti-inflammatory drugs and other anthranilic acids inhibit the Na^+/dicarboxylate symporter from *Staphylococcus aureus*. *Biochemistry* **52**, 2924–2932 (2013).

ONLINE METHODS

Model building. A VcINDY outward-facing model was obtained by applying the repeat-swapped homology modeling technique according to a recently updated protocol[26] . The repeats in the VcINDY structure, PDB 4F35, were defined as comprising residues 42–242 for repeat unit 1 (RU1) and 253–462 for repeat unit 2 (RU2). TM-align was used to structurally superimpose these repeats[43], thus yielding template modeling scores (TM scores), which provide a measure of structural similarity that is independent of segment length (values between 0 and 1, with 1 being structurally identical). The obtained TM scores supported the r.m.s. deviations reported in Results; specifically, superimposing the entirety of each repeat yielded a TM score of 0.52, which increased to 0.78 and 0.83 when only the transport and scaffold domain helices, respectively, were compared. The analysis of the symmetry axis of the repeats was performed with SymD[44]. An initial sequence alignment of the template and the model sequences was compiled from the TM-align output. This initial alignment was refined by removing gaps within secondary-structural elements (obtained from DSSP[45,46]) and by using conservation scores (obtained from the ConSurf server with default settings[47]) to position conserved residues so that they were preferentially oriented toward the inside of the protein. After each adjustment to the alignment, 200 iterations of restraint optimization were performed with MODELLER v9.13 (ref. 48) to verify whether the resultant models exhibited improvements in MolPDF and ProQM[49] scores as well as Procheck analysis[50].

The refined final alignment (**Supplementary Fig. 1**) was then used to generate a set of 2,000 repeat-swapped 3D models of which the best model was selected as that which best met the following criteria: the lowest MolPDF score, the highest global ProQM score, and the most residues in favored regions of the Ramachandran plot. This model was then used to identify the scaffold and transport domains, which were assigned as residues 19–126 plus 253–356, and 127–242 plus 357–462, respectively. Final refinement of the model involved adding distance restraints between Cα atoms taken from the known structure in addition to those necessary to position the ions and bound ligand in the binding site. Distance restraints between Cα atoms were assigned according to the input crystal structure for all pairs of Cα atoms <60 Å apart within either the transport or scaffold domains in the template structure, PDB 4F35. We note that these intradomain restraints did not alter the extent of the conformational movement but maintained the internal arrangement of the two domains (**Supplementary Figs. 2b** and **7**). Distance restraints were also applied in the substrate-binding sites: between the Na^+ ion and the O atoms in the backbones of S146, S150 and N199, the hydroxyl group of S146 and the amide group of N151; and between any nonhydrogen atoms of the substrate mimic (citrate) and the protein within 3.5 Å in the template structure. All applied distance restraints were represented as Gaussians with an s.d. of 0.1 Å. With these restraints, a new set of 2,000 models was generated with MODELLER, and again the final model was chosen on the basis of the criteria mentioned above.

The orientation of the VcINDY X-ray structure in the membrane was determined with the OPM server[51]. The orientation of the protomer model was defined after superposition of the scaffold domain onto that of the crystal structure. A dimeric model was constructed by superposing the same model onto both protomers in the crystal structure, and MODELLER was used to locally refine residues in the interface, defined as any residues containing an atom within 5 Å of the other protomer in the model after superposition (residues 63–113 of TM3–TM4b and residues 286–339 of TM8–TM9b). The r.m.s. deviation of the refined dimer model compared to the initial dimer model was 0.17 Å over all atoms. For the analysis of the transport-scaffold interface, we selected all residues with any atom within 5 Å of the other domain in either the inward- or outward-facing conformation. All molecular figures and movies were generated with PyMOL (http://www.pymol.org/) unless stated otherwise. The final outward-facing VcINDY model has been deposited in the Protein Model Database[52] under identifier PM0080216.

Molecular biology and cysteine-mutant design. All mutants were made with a QuikChange II site-directed mutagenesis kit (Agilent Technologies) and were fully sequenced to ensure sequence fidelity. All cysteine mutants were generated in a cysteine-free background in which all three native cysteines in VcINDY were substituted for serine.

In total, we introduced 18 different combinations of double-cysteine mutants into the interface between the transport and scaffold domains. However, most of these mutant combinations resulted in unstable protein that expressed poorly or aggregated (**Supplementary Table 1**). The majority of these cysteine substitutions were located toward the center of the transport domain in positions with low solvent accessibility. Only one of the buried interfacial pairs that we tested, T154C V272C, yielded stable protein and was used in further studies (**Fig. 2b**). The distance between the Cβ atoms of T154 (from HP1) and V272 (from TM7) in the inward-facing structure (d_{ifs}) was 18.7 Å, whereas in the outward-facing model the distance (d_{ofm}) was 3.9 Å. We subsequently targeted regions at the periphery of the interface, particularly the symmetry-related helices 4c and 7c. Solvent-accessible loops were more tolerant to modification, and hence we were able to introduce two cysteine pairs, A120C V165C, in helix 4c/HP1 (d_{ifs} = 11.7 Å; d_{ofm} = 4.7 Å) and A346C V364C in helix 9c/HP2 (d_{ifs} = 16 Å; d_{ofm} = 5.6 Å), with no apparent reduction in protein stability (**Fig. 2b**). For the inward-facing control mutant, L60C S381C, d_{ifs} = 6.9 Å; d_{ofm} = 20.6 Å.

Protein expression and purification. VcINDY and its variants were expressed and purified as detailed previously. VcINDY was expressed in *E. coli* BL21-AI cells (Life Technologies) from a modified pET vector in frame with an N-terminal decahistidine tag[53]. Cells were grown in LB supplemented with 30 μg/ml kanamycin at 37 °C until they reached an A_{600} of 0.8, at which point they were rapidly cooled to 19 °C in an ice bath. Expression was induced by addition of IPTG and L-arabinose to final concentrations of 10 μM and 6.6 mM, respectively. Cells were incubated overnight at 19 °C. Cells were harvested and resuspended in lysis buffer (50 mM Tris, pH 8, 400 mM NaCl and 20% glycerol), and lysed with a homogenizer (Emulsiflex-C3, Avestin). The membrane fraction was isolated by ultracentrifugation, resuspended in purification buffer (50 mM Tris, pH 8, 200 mM NaCl and 10% glycerol) and solubilized by addition of *n*-dodecyl-β-D-maltoside (DDM, Anatrace) to a final concentration of 20 mM. Residual insoluble material was removed by ultracentrifugation, and the soluble fraction was incubated with Talon metal-affinity resin (Takara Bio) overnight at 4 °C. Resin was washed by consecutive additions of 20 column volumes of 10 mM and 20 mM imidazole-containing purification buffer supplemented with 2 mM DDM. Bound protein was eluted while the affinity tag was simultaneously cleaved by incubation of the resin with purification buffer supplemented with 2 mM DDM and 10 μg/ml trypsin at 4 °C for 1 h. The flow through from the column was collected, concentrated and further purified with a Superdex 200 SEC column (GE Healthcare) equilibrated with SEC buffer (25 mM Tris, pH 8.0, 100 mM NaCl, 5% glycerol and 3% *n*-decyl-β-D-maltoside (DM)). For the dimer-interface mutants, protein was eluted from the Talon resin by addition of purification buffer supplemented with 300 mM imidazole. The affinity tag was maintained for identification of the protein with western blotting. The dimer-interface mutants were then desalted into SEC buffer with Zeba Spin desalting columns (Life Technologies). Purified protein was concentrated, snap frozen and stored at −80 °C. All proteins were purified with buffers containing either 0.5 mM Tris(2-carboxyethyl)phosphine (TCEP) or 1 mM DTT to keep the cysteines reduced. For detection of histidine-tagged protein, western blotting was used with anti-pentahistidine antibody (Qiagen cat. no. 34660; validation provided on the manufacturer's website).

Reconstitution. The functional reconstitution of protein into liposomes was performed as described previously[54]. 25–100 μg of purified protein was diluted to 2 ml in SEC buffer (with 1 mM DTT if required) and mixed with 400 μl 20 mg/ml lipids, which consisted of a 3:1 mixture of *E. coli* polar lipids and POPC (Avanti Polar Lipids). The protein/lipid mixture was incubated on ice for 10 min and then rapidly diluted into 65 ml inside solution containing 20 mM Tris/HEPES, pH 7.5, 1 mM NaCl, 199 mM KCl and 0.5 mM TCEP/1 mM DTT when required. Proteoliposomes were collected by ultracentrifugation and resuspended in inside solution to a concentration of 8 mg/ml lipid. Proteoliposomes were freeze-thawed three times and stored at −80 °C or used immediately. After this point, the internal solution was modified by collecting the proteoliposomes by centrifugation, resuspending them in the desired solution, freeze-thawing three times and extruding.

***In vitro* transport assays.** Proteoliposomes were prepared for transport assays by extrusion through a 400-nm filter 11 times and were concentrated to 80 mg/ml lipid with ultracentrifugation. The transport assays were started by addition of the proteoliposomes to reaction buffer (20 mM Tris/HEPES, pH 7.5, 100 mM NaCl, 100 mM KCl, 1 μM valinomycin, and 1 μM [^{3}H]succinic acid (American

Radiolabeled Chemicals). At the indicated times, samples were collected, and the reaction was terminated by addition of the sample into ice-cold quench buffer (20 mM Tris/HEPES, pH 7.5, and 200 mM ChCl) and rapid filtration through a 200-nm nitrocellulose filter (Millipore). The filter was washed with 3 ml quench buffer, the filters were dissolved in FilterCount liquid scintillation cocktail (PerkinElmer) and the [^{3}H]succinic acid internalized by the proteoliposomes was counted with a Trilux beta counter (PerkinElmer).

Protein cross-linking and PEGylation assay. To induce disulfide-bond formation in detergent-solubilized protein (as in the band-shift assay), the proteins were exchanged into conjugation buffer (50 mM Tris, pH 7, 100 mM NaCl, 5% glycerol, and 3% (w/v) DM) with Zeba Spin Desalting Columns (Thermo Fisher Scientific) to remove the reducing agent and then were incubated with a five-fold molar excess of $HgCl_2$ or freshly prepared solution of copper phenanthroline (CuPhen). A 2:1 ratio of CuPhen was prepared by mixing solutions of 500 mM 1,10-phenanthroline and 250 mM $CuSO_4$. The final CuPhen concentration ranged from 10 to 500 µM depending on the particular cysteine mutant. Regardless of which cross-linking reagent was being used, the cross-linking reaction was incubated at room temperature for 45 min. Control samples were treated identically except for incubation in the presence of 0.5 mM TCEP or 1 mM DTT. After this incubation, the cross-linker was removed by exchanging the protein into conjugation buffer containing no cross-linking agent. To PEGylate any free cysteines, the protein samples were then incubated for 3 h at room temperature in the presence of 0.5% (w/v) SDS and 2 mM mPEG5K. Proteins were separated on nonreducing 12% polyacrylamide gels, which were stained with Coomassie dye to visualize the protein.

Cross-linking the proteins already incorporated into liposomes was achieved by addition of 50 µM $HgCl_2$ to the liposome suspension. To facilitate internalization of the $HgCl_2$, the treated proteoliposomes underwent three freeze-thaw cycles and were extruded through a filter with an 0.4-µm pore size. After freeze-thaw treatment and extrusion, the liposomes were incubated for 30 min at room temperature. $HgCl_2$ was removed by exchanging the solutions on both sides of the membrane for inside buffer. This exchange was performed by pelleting of the proteoliposomes by ultracentrifugation and resuspension in the desired buffer. At this stage, 1 mM DTT was added when appropriate. Solutions were equilibrated across the membrane, again by three freeze-thaw cycles and extrusion. Original images of gels and blots used in this study can be found in **Supplementary Data Set 1**.

Unexpectedly, cysteineless VcINDY showed less activity in the presence of Hg^{2+} than under reducing conditions (**Fig. 5**); however, this effect actually reflects an enhancement of activity due to the reducing agent, DTT (**Supplementary Fig. 6c**). Indeed, the presence of increasing amounts of $HgCl_2$ actually increased the cysteineless protein's transport activity (**Supplementary Fig. 6d**).

Protein digestion and mass spectrometry. Protein samples, at 10 µM, in 50 mM Tris, pH 7, 150 mM NaCl, 5% glycerol, and 0.1% DM were either reduced with 1 mM DTT (R) or treated with 100 µM or 500 µM CuPhen to induce disulfide formation (X); this was followed by desalting to remove the reagent. ~5 µg of protein was alkylated by incubation with 10 mM *N*-ethylmaleimide (NEM, Sigma) for 20 min at room temperature. A120C V165C was digested with 500 ng trypsin for 8 h at 37 °C and further digested with 300 ng chymotrypsin (Roche) for 8 h at 25 °C; T154C V272C was digested with 600 ng chymotrypsin at 25 °C overnight. The digests were cleaned with an HLB µElution plate (Waters). The LC/MS/MS experiments were performed on an Orbitrap Elite mass spectrometer (Thermo Scientific) connected to a 3000 RSLC nano HPLC system with an RS autosampler (Thermo-Dionex) via an Easy-Spray ion source (Thermo Scientific). Approximately 1 µg of digested protein was injected onto an ES802 Easy-Spray column (25 cm × 75 µm ID, PepMap RSLC C18 2 µm; Thermo Scientific) and then separated at a flow rate of 300 nl/min with a 38-min linear gradient of 2–30% mobile phase B (mobile phase A, 2% acetonitrile and 0.1% formic acid; mobile phase B, 98% acetonitrile and 0.1% formic acid).

The Orbitrap Elite was operated in decision-tree mode. The precursor ion scan was performed in the Orbitrap with a resolution of 60 K at m/z of 400. The m/z range for survey scans was 300–1,600. The fragment-ion scan was performed in the linear ion trap. The minimum signal threshold for MS/MS scans was set to 3×10^4, and up to 10 MS/MS scans were performed after each MS scan. A 9-s dynamic exclusion window was selected with early expiration enabled.

Peptide identification. Mascot Distiller (version 2.5.1.0) was used to convert the Xcalibur Raw data to a peak list file in MGF format. Mascot Daemon 2.4.0 was used to submit the MGF files to Mascot Server 2.4 for the database search. Data were searched against a house-built database that contains the sequences of the NCBI human database and the sequences of A120C V165C, T154C V272C, and A346C V364C. The following parameters were included in the search: peptide tolerance, ± 10 p.p.m.; MS/MS tolerance, 0.2 Da; instrument type, CID+ETD; enzyme, none; missed cleavage, 0; variable modifications, oxidation (M) and NEM (C). Once a peptide (Px) containing a cysteine residue was detected, a second database search was performed, assuming Px – 2H (the mass of Px minus two hydrogen atoms) as a potential modification. Once a plausible cross-linked candidate was found in the second search, the MS/MS spectrum of that candidate was manually checked. A potentially cross-linked candidate was considered to be real if the following conditions were satisfied: (i) major peaks of the MS/MS spectrum of the cross-linked candidate could be assigned manually and (ii) the candidate was detected in only the X samples and not in the corresponding R samples.

43. Zhang, Y. & Skolnick, J. TM-align: a protein structure alignment algorithm based on the TM-score. *Nucleic Acids Res.* **33**, 2302–2309 (2005).
44. Tai, C.H., Paul, R., Dukka, K.C., Shilling, J.D. & Lee, B. SymD webserver: a platform for detecting internally symmetric protein structures. *Nucleic Acids Res.* **42**, W296–W300 (2014).
45. Edgar, R.C. Quality measures for protein alignment benchmarks. *Nucleic Acids Res.* **38**, 2145–2153 (2010).
46. Kabsch, W. & Sander, C. Dictionary of protein secondary structure: pattern recognition of hydrogen-bonded and geometrical features. *Biopolymers* **22**, 2577–2637 (1983).
47. Ashkenazy, H., Erez, E., Martz, E., Pupko, T. & Ben-Tal, N. ConSurf 2010: calculating evolutionary conservation in sequence and structure of proteins and nucleic acids. *Nucleic Acids Res.* **38**, W529–W533 (2010).
48. Sali, A. & Blundell, T.L. Comparative protein modelling by satisfaction of spatial restraints. *J. Mol. Biol.* **234**, 779–815 (1993).
49. Ray, A., Lindahl, E. & Wallner, B. Model quality assessment for membrane proteins. *Bioinformatics* **26**, 3067–3074 (2010).
50. Laskowski, R.A., Macarthur, M.W., Moss, D.S. & Thornton, J.M. Procheck: a program to check the stereochemical quality of protein structures. *J. Appl. Cryst.* **26**, 283–291 (1993).
51. Lomize, M.A., Lomize, A.L., Pogozheva, I.D. & Mosberg, H.I. OPM: orientations of proteins in membranes database. *Bioinformatics* **22**, 623–625 (2006).
52. Castrignanò, T., De Meo, P.D., Cozzetto, D., Talamo, I.G. & Tramontano, A. The PMDB Protein Model Database. *Nucleic Acids Res.* **34**, D306–D309 (2006).
53. Love, J. *et al.* The New York Consortium on Membrane Protein Structure (NYCOMPS): a high-throughput platform for structural genomics of integral membrane proteins. *J. Struct. Funct. Genomics* **11**, 191–199 (2010).
54. Mulligan, C. *et al.* The substrate-binding protein imposes directionality on an electrochemical sodium gradient-driven TRAP transporter. *Proc. Natl. Acad. Sci. USA* **106**, 1778–1783 (2009).

doi:10.1038/nsmb.3166